Technology

Polymers

Observation of microphase segregation in binary polymer brushes
Usov, D., C. Froeck, A. Scholl, S. Minko, M. Stamm

Optimization of PEEM-2 for studies of organic thin film
Morin, C., A.P. Hitchcock, H. Ikeura-Sekiguchi, A. Scholl, A. Doran, K. Kaznacheyev

Orientation of fibrils in polymer crazes studied by STXM
Koprinarov, I., M. Demirors, T. Tyliszczak, D. Kilcoyne, A. Hitchcock, H. Ade, R. Cieslinski, G. Mitchell

Resonant small angle x-ray scattering of polymers at the C-K edge
Koprinarov, I., G. Mitchell, B. Landes, M. Devon, J. Kortright

Spectroscopic observation of polaron-lattice band structure in the conducting polymer polyaniline
Kurmaev, E.Z., M.I. Katsnelson, A. Moewes, M. Magnuson, J.-H. Guo, S.M. Butorin, J. Nordgren, D.L. Ederer, M. Iwami

Status of the 5.3.2 bend magnet polymer STXM
Kilcoyne, D., H. Ade, T. Tyliszczak, A.P. Hitchcock, E.G. Rightor, G.E. Mitchell, M. Kritscher, T. Warwick, K. Franck, E. Anderson

X-ray spectromicroscopy of branched polyolefin blends
Appel, G., I. Koprinarov, G.E. Mitchell, A.P. Smith, H. Ade

Observation of microphase segregation in binary polymer brushes

D. Usov[1], C. Froeck[1], A. Scholl[2], S. Minko[1], M. Stamm[1]
[1]Institut for Polymer Research Dresden, Hohe St. 6, 01069 Dresden, Germany
[2]Advanced Light Source, Ernest Orlando Lawrence Berkeley National Laboratory,
University of California, Berkeley, California 94720, USA

INTRODUCTION

The basic idea is creation of smart polymer layers with switching properties such as wetting behavior, adhesion, interaction with biological objects, and permeability of membranes. Such polymer layers can find their application in many areas such as information recording, sensors, self-cleaning clothes covering, nanodevices, in medicine and biological science for mimicking living cell membranes, for selective adsorption and recognition of proteins and living cells. The route, how to make this dream true, comprises binding to solid substrate different polymers[1] or block-copolymers and switch the film structure in such a way, that this film responding to various external stimuli can adopt particular desired properties: hydrophylic/hydrophobic balance, selective adsorption of particular molecules, etc.

We are currently studying model layers composed of two different (hydrophilic and hydrophobic) linear polymers covalently grafted to silicon substrates which can be switched upon exposure to solvents of different thermodynamical quality[1]. The grafting density is so high that the distance between grafting points of neighbor polymer molecules is much (about 10 times) shorter than the size of the polymer coils (mean distance between chain ends in theta-conditions). Therefore the polymer coils interact with their neighbors and are elongated in the direction perpendicular to the substrate. All the conformational changes are cooperative. Such regime is known as the brush regime. If such a binary polymer brush is exposed to a selective solvent which good for the first brush polymer and poor for the second one the first polymer swells and occupies the top layer while the second polymer collapses and occupies the bottom layer near the substrate. If the solvent is replaced by another one with opposite selectivity the brush passes to a state inverse with respect to the previous one. In a solvent good for both polymers they both are present on the top of the layer. The time of solvent evaporation upon drying by nitrogen flow is much smaller than the time for morphology transformation. The morphologies after treatment in a particular solvent are reproducible and reversibly switch upon changing the solvent. We made the assumption that the spacial distribution of the polymers in the dry state after exposition to a solvent is a fingerprint of their distribution under the solvent[2].

The polymers are usually incompatible but only microphase segregation takes place because each polymer chain is chemically bound to a substrate with one end. The size of the aggregates is limited by the chains` length. Two limiting types of morphologies can be distinguished: the layered phase with only perpendicular phase segregation and the “ripple” phase with lateral segregation. Analytical studies of the microphase segregation in binary brushes under melt conditions and in various solvent conditions were done. Self consistent field calculations made by Marcus Müller[2] predict for binary polymer brushes in a solvent good for both components existence of the “ripple” phase consisting of parallel lying cylinders with alternating enrichment by each brush component. For the case of a selective solvent an existence of the “dimple” phase is predicted where the worse soluble polymer forms round clusters and the other polymer occupies the area around them. Experimental observation of microphase segregation in binary

polymer brushes was performed using facilities of the Ernest Orlando Lawrence Berkeley National Laboratory and was briefly reported elsewhere[2].

RESULTS

We synthesized binary polymer brushes by radical polymerization on a Si surface using for the grafting of the second polymer the residual azo-initiator on the surface[1]. The brush components were polystyrene with 25% of fully fluorinated aromatic rings (P(S-co-FS)) and polymethylmethacrylate (PMMA).

We observed the reversible morphology switching from elongated species after treatment in toluene to round clusters after exposition to acetone with Atomic Force Microscopy (AFM) (see Fig.1).

We investigated the chemical composition of the brushes` top layers (≤5 nm) after exposition to toluene and acetone applying X-Ray Photoelectron Emission Microscopy (XPEEM). The difference between the carbon peaks in Near Edge X-Ray Absorption Fine Structure spectra (NEXAFS) for polystyrene (286.1 eV) and PMMA (289.3 eV)[3] was used to distinguish between the polymers. We observed the inverse contrast of elongated species at the XPEEM images recorded at 286.1 eV and 289.3 eV for the brush exposed to toluene (see Fig.2). We were unable to find any chemical contrast at the XPEEM images for the brush exposed to acetone due to a strong signal distortion caused by highly rough brush surface.

The integral NEXAFS spectra were recorded from the surfaces of the brushes after exposure to toluene, acetone, and after annealing at 150ºC for 24 hours in vacuum. The water contact angle on the same surfaces was measured. The chemical composition of the top layers of the brushes was calculated and similar results were obtained from these two methods. The top layer of the brushes was enriched with P(S-co-FS) after exposition to toluene and after annealing and with PMMA after exposition to acetone (see Table 1).

We conclude qualitative agreement of the experimentally observed morphologies with the self consistent field calculations.

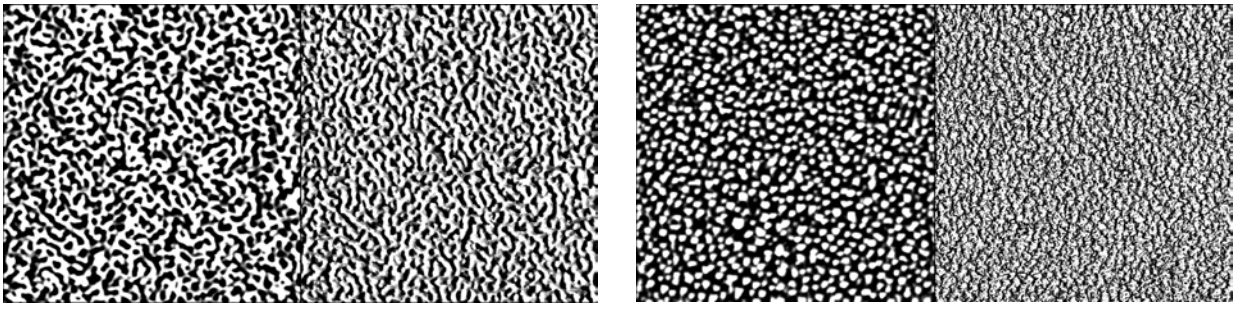

Figure 1. AFM tapping mode images 5x5 μm of the P(S-co-FS)/PMMA brush after exposure to toluene (A,B) and acetone (C,D): topography (A,C), phase (B,D) at 50% set-point ratio.

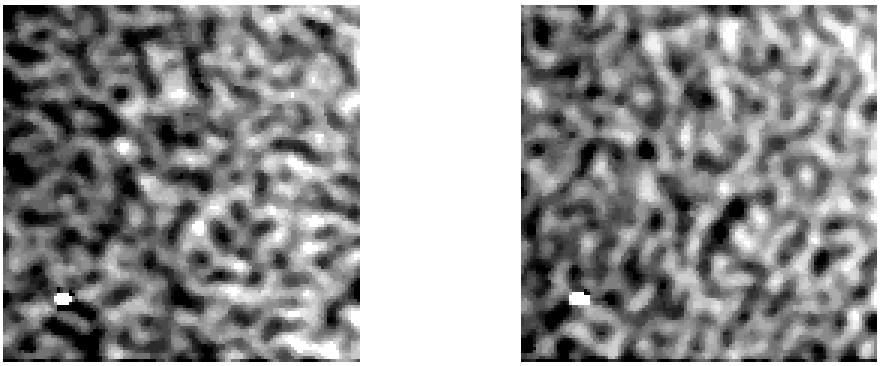

A B

Figure 2. XPEEM images 3x3 μm of the PSF-PMMA1 brush after exposure to toluene showing contrast between C edges of both polymers at 286,1 eV (A) and 289,2 eV (B) for PS and PMMA, respectively.

Table 1. Fraction of PMMA in the top layer of the brushes after exposure to solvents and annealing.

Sample	Contact angle, deg	PMMA fraction in the top layer, % calculated from the contact angle	PMMA fraction in the top layer, % calculated from the XPEEM data
P(S-co-FS)	96.6	0	0
PMMA	76.1	100	100
P(S-co-FS)/PMMA brushes after:			
exposure to toluene	90	32	29
exposure to acetone	81	76	78
in vacuum, at 150°C for 10h	91.5	25	20

REFERENCES

1. Alexander Sidorenko, Sergiy Minko, Karin Schenk-Meuser, Heinz Duschner, and Manfred Stamm, *Langmuir*, Vol. 15, N 24, **1999**, p. 8349.
2. S. Minko, M. Müller, D. Usov, A. Scholl, C. Froeck, and M. Stamm, *Physical Review Letters*, Vol. 88, N 3, **2002**, 035502.
3. Adam Hitchcock, McMaster University, 1280 Main Street West, Hamilton, Ontario, L8S 4L8, Canada, E-mail: aph@mcmaster.ca, private communication.

This work was supported by the Institute for Polymer Research Dresden, Hohe St. 6, 01069 Dresden, Germany and the European Graduate College "Advanced Polymeric Materials", Technical University Dresden, 01062 Dresden, Germany.

Principal investigator: Manfred Stamm, Institute for Polymer Research Dresden, Hohe St. 6, 01069 Dresden, Germany, E-mail: stamm@ipfdd.de, tel. +49 (351) 4658 224, web site: www.ipfdd.de.

Optimization of PEEM-2 for studies of organic thin films

C. Morin[1], A.P. Hitchcock[1], H. Ikeura-Sekiguchi[1,2], A. Scholl[3], A. Doran,[3] K. Kaznacheyev[4]
[1]BIMR, McMaster University, Hamilton, ON, Canada L8S 4M1
[2]Quantum Radiation Division, Advanced Industrial Science and Technology (AIST), Tsukuba, 305-8568 JAPAN
[3]Advanced Light Source, Berkeley Lab, Berkeley, CA 94720
[4]Physics, CLS, University of Saskatchewan, Saskatoon, SK Canada S7N 5C6

INTRODUCTION

There are many potential applications of X-ray photoelectron emission microscopy (X-PEEM) to organic thin films, such as fundamental studies of phase separation [1], and applied studies of organic light emitting diodes, adhesion promoters [2] etc. In order to obtain meaningful results, it is important to understand the challenges of applying X-PEEM to organics, and to develop compensating data acquisition strategies. These challenges include: radiation damage, camera artifacts, Io determination, higher order radiation, charging, sample damage from field emission or discharges.

The photon flux at BL 7.3.1 ($>10^{12}$ photons/s at 500 eV in a 30x300 μm spot, with 1.9 GeV, 400 mA) is very high because there are only two optical elements and energy resolution is sacrificed for flux. The high flux, combined with a relatively inefficient electrostatic column (~5 % transmission at high spatial resolution – 12 μm aperture) and an inefficient camera, mean that ratio of detected signal to number of photons absorbed in the near surface region is very small. In order to perform useful chemical analysis, images of the region of interest must be recorded at a number of energies (in the C1s, N1s or O1s regions for organic samples) to form an image sequence which can be subsequently analysed to obtain point or region spectra, or chemical maps. Other problems occur because of limitations of the CCD camera - bad pixels; pixel-to-pixel variation in dark signal (leakage) and gain; as well as a slow data transfer rate (0.25s/image, no ability to transfer sub images). A further challenge is the uneven illumination in the PEEM; in order to gain sensitivity we use reduced magnification. Typically the camera views 60x60 μm^2 but only the central third of the image is illuminated.

In order to reduce the damage rate we work at much reduced flux, achieved by placing an aperture (formed by two independently adjustable elements, called 'chopper' and 'mask') in the beam before the monochromator. This reduces the energy resolution as well as the flux – at a chopper value of 15 the resolving power is only 100. Under typical low dose conditions we work with less than 10% of the dynamic range of the camera. Background and camera corrections are extremely challenging. It is essential to record Io spectra from a suitable reference surface, typically HF-etched silicon for organic thin film samples deposited on Si or Si_3N_4. This is especially true in the C 1s region where there is a lot of structure in the Io spectrum. The Io signal must be measured under very similar conditions to those used to study the sample in order to ensure the same sensitivity, energy resolution and higher order content, (the latter two depend on the exact choice of chopper, windows, slits and filters used). The PEEM sensitivity is very dependent on the sample-objective lens distance, which changes every time a sample is re-positioned.

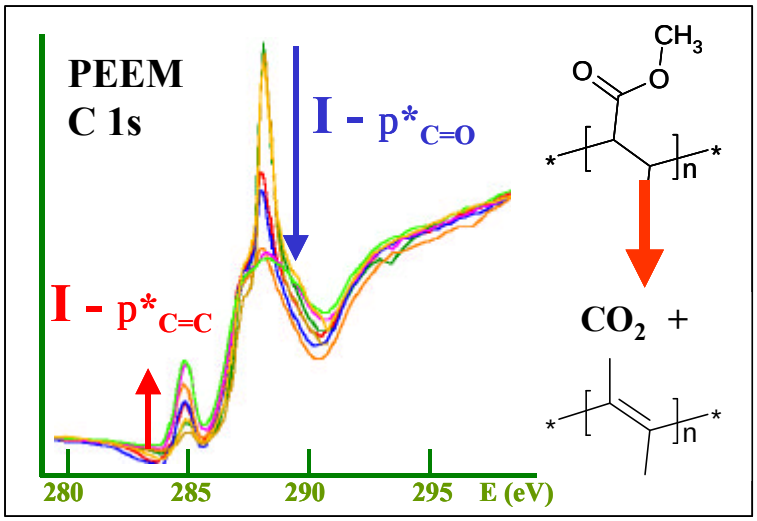

Fig. 1 Plots of C 1s NEXAFS of a 50 nm PMMA film on c-Si. Successive scans made on the same spot build up dose and damage.

Charging can occur for any insulating sample, although it is often surprising the samples that can be studied by PEEM. We typically observe charging if a polymer sample is too thick (> 75 nm), or too corrugated (> 15 nm rms). In some cases a thin metal coating (<2-3 nm) can be evaporated to control charging. Charging results in dark spots on images, where the electrons are trapped by the surface charge potential, or in bright spots, where there is artificially enhanced emission by discharges or, at locations of high curvature, by enhanced detection

probability due to stronger fields. While it is sometimes possible to record meaningful NEXAFS spectra from charging surfaces, more typically, charging results in large and variable sample or objective lens currents which lead to unstable operation, and, in extreme cases, macroscopic discharges that can damage samples, making dramatic dendritic patterns in organic layers, and exploding Si_3N_4 windows. In the following we describe a systematic study of a pure polymethylmethacrylate (PMMA) film in order to characterize its radiation damage rate, and thereby develop procedures to study heterogeneous samples containing PMMA in a meaningful fashion, despite these challenges. A detailed manual for operating X-PEEM and choosing parameters optimal for radiation sensitive samples is available at the beam line or from the authors [3].

EXPERIMENTAL

~50 µl of a 1.0% w/w toluene solution of PMMA (Mw = 112.3 K, Mw/Mn = 1.09, Polymer Source Inc) was passed through a teflon filter to remove particulate impurities and dropped onto a spinning HF-etched Si chip at 4000 rpm. Spinning was continued for ~5 s. The film thickness was estimated to be ~40 nm from AFM at a scratch and the rms roughness was 6 nm The sample was not annealed.

Property	Value	Property	Value
Mask	0.9	Dwell (s)	3
Chopper	15 or 16	Camera gain	normal, x8
Al window #1	in	PEEM aperture (µm)	50
Al window #2	in	Sample (kV)	18.0
Exit slit	in	Objective (kV)	13.68
Ti filter (150 nm)	in	Transfer (kV)	12.45
Flash light	on	Intermediate	13.78
Background (Hz)	50	Projection	0

The relationship of measured intensity to the various parameters controlling the signal is summarized in **equation 1**. A number of scale factors need to be determined but this qualitative formula may be useful for others using PEEM-2 for organic thin film studies.

$$S = G*t*[I*\sigma*f_{esc}*F*\varepsilon_{PEEM} - B] \quad \text{(eqn 1a)}$$

where S = detected signal , G = camera gain (2,4,8), t = time, σ = cross-section, f_{esc} = electron escape probability (integrated over inelastic scattering and angular effects), F = work function, ε_{PEEM} = PEEM column efficiency [α (magnification)* (aperture)^2], B = no-X-ray background, and I is the flux (ph/s) on the sample, given by

$$I \alpha\ I_{ring}*C*T \quad \text{(eqn 1b)}$$

where C, the chopper factor is $(C_{max}-C)/C_{max}$; and T, the Ti filter factor, is $(T_{max}-T)/T_{max}$.

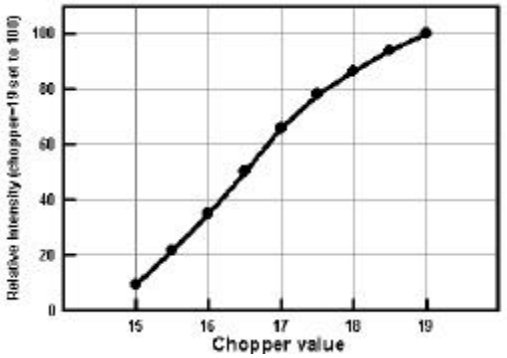

Fig. 2 Variation of flux on sample vs. chopper.

RESULTS AND DISCUSSION

Fig. 1 shows a typical sequence of spectra (without Io correction) recorded while the sample was being damaged. The relative radiation damage rate for PMMA in the low dose regime was determined by recording successive image sequences on the same spot, using the instrumental parameters listed in table 1. Only 24 energies in 283-295 eV range were used in order to track damage changes adequately. In general keeping the number of sampled energies to the minimum is a key step in making meaningful measurements of organics. The *relative dose* was obtained from the integrated spectral signal up to a given measurement, taking into account the dead time between images (~2 s). The *relative damage* was obtained from the increase in the area of the 285 eV $\pi^*_{C=C}$ peak (growth of reduced sites in the backbone) and decrease in the area of the 288 eV $\pi^*_{C=O}$ peak (loss of acrylate groups). In addition to the measurements made at low dose, another series at much higher dose (5 or 10 s exposure at chopper 19) was performed. The two sets were matched in the overlapping region of the 285 eV and 288 eV damage curves. Finally the dose scale was expressed in terms of time equivalent at full flux in the carbon 1s region using the variation of signal strength with chopper setting to scale the times (**Fig. 2**).

Fig. 3 plots damage versus relative dose for PMMA as measured in the PEEM As is typical in radiation damage curves, there is an exponential change with saturation. Based on these results, we estimate that, at the full flux dose rate (chopper = 19, 400 mA in the ALS), the total acceptable exposure time for meaningful measurements of samples containing PMMA with negligible damage (as measured by spectral change) is 10 seconds. Since it takes about 5 seconds to record an image of acceptable quality, if full flux is used it is only possible to record a few images before the PMMA in a PMMA-containing sample is irreversibly modified. We note that a recent study of radiation damage in various polymers by STXM [4] indicates that PMMA is about average in terms of radiation sensitivity.

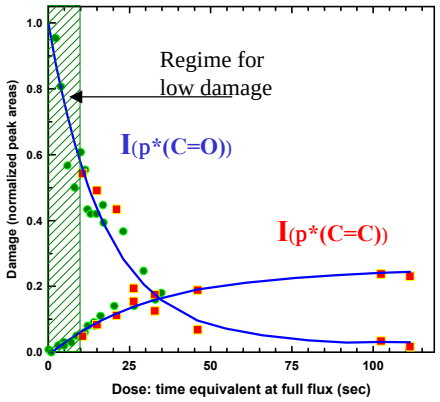

Fig. 3 Intensity at 288 eV and 285 eV versus accumulated radiation dose. The dose is time to equivalent deposited energy when PEEM is operated with full flux. The green points are measurements made at reduced flux. Chopper: green (15), red (19).

Chemical imaging with PEEM requires images at a number of energies.Typically 10-15 images are needed. The only way to get these without "frying the sample" is to "turn down the torch". We routinely do this by using the chopper to reduce the flux ~10-fold (see Fig. 2). This allows 10-20 images to be recorded prior to significant damage. Chopper values below 15 are not useable since the grating is inadequately illuminated. 2-bunch mode is also useful, but normalizing the rapid time variation of flux is a challenge.

Fig. 4 presents results of a low dose study of a 20:80 (w/w) PS:PMMA film (PS = polystyrene) which has domain sizes on the order of 250 nm as determined by prior AFM measurements. This is a continuation of our earlier studies of phase segregation on PS:PMMA blends [1]. We are trying to develop a metastable system with flat, reasonably large domains that are pure PS and PMMA, in order to carry out competitive protein adsorption studies. As the analysis of the spectrum of the PMMA-rich regions shows, the as-made material still contains significant PS, as found earlier [1]. However, with our refined understanding of the damage rate of PMMA in PEEM-2, we are now very confident that the 285 eV signal observed in the PMMA-rich domains is from incompletely phase segregated PS and NOT from the C=C bonds formed from radiation damage of PMMA (Fig 1).

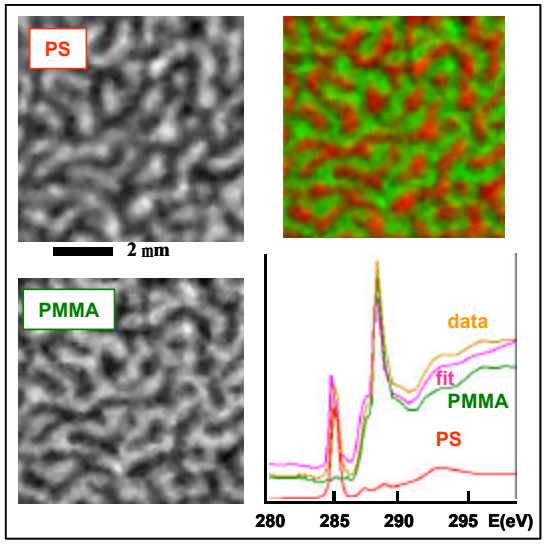

Fig. 4 PS and PMMA component maps, and color composite derived from image sequence of as-made 20:80 PS:PMMA blend, using low dose protocol (3s dwell, chopper=16, few points). Lower right shows the results of a curve fit to the spectrum of pixels in strong PMMA regions. (Jun-01).

SUMMARY: Relative dose - damage relationships for PMMA were measured in PEEM-2 to define an acceptable regime [5]. Similar calibration measurements are required prior to study of other radiation sensitive samples. Self-assembled monolayer and micro-contact printed systems involving fluorocarbons are particularly challenging due to their very small thickness (< 5nm) and extreme radiation sensitivity. An even more rigorous application of the methods outlined in this report is required for successful studies of such materials.

1. C. Morin et al, *J. Electron Spectrosc* 121 (2001) 203-224
2. G. E. Mitchell, et al. 1999 ALS Compendium (2000)
3. C. Morin, A.P. Hitchcock, H. Ikeura-Sekiguchi, A. Doran and A. Scholl, PEEM-2 manual (2001).
4. T. Coffey, S.G. Urquhart and H. Ade, *J. Electron Spectroscopy* 122 (2002) 65.
5. C. Morin, A.P. Hitchcock, et al in preparation.

Supported by NSERC (Canada) and Canada Research Chair program. ALS is supported by U.S. DoE (DE-FG02-89ER60858). Data analysis done with **aXis2000**, an IDL widget available at http://unicorn.mcmaster.ca/aXis2000.html

Principal investigator: *Adam Hitchcock*, McMaster, **aph@mcmaster.ca**. Ph: 905 525-9140

Orientation of fibrils in polymer crazes studied by STXM

Ivo Koprinarov[1], Mehmet Demirors[2], Tolek Tyliszczak[1], David Kilcoyne[3], Adam Hitchcock[1], Harald Ade[3], Robert Cieslinski[2] and Gary Mitchell[2]
[1]BIMR, McMaster University, Hamilton, ON, L8S 4M1 Canada
[2]The Dow Chemical Company, Building 1897 E, Midland MI 48667, USA
[3]Physics, North Carolina State University, Raleigh, NC, USA

INTRODUCTION

Many important thermoplastic polymers are very brittle in their neat form and thus one of the most important areas of endeavour for the polymer scientist is to improve and control the toughness of common polymeric systems. An understanding of the fundamental fracture mechanics of polymers should facilitate the design of tougher materials. Failure of brittle polymers generally occurs by crack formation. The crack begins as a craze, in which the separating polymer surfaces are bridged by small filaments or fibrils of polymer. The fibrils are formed as polymer molecules are pulled out from the bulk material. One would presume that the polymer chains would be strongly aligned along the fibril direction. Knowledge of the degree of orientation prior to break and the variation of this property for different size crazes, and different materials will provide data important to any mathematical model of polymer deformation. If reliable, such a model could be used to design better materials. However, until now the quantitative data at high spatial resolution needed to test any proposed model has not been accessible by any known method. The enhanced spatial resolution and improved stability of the new scanning transmission x-ray microscope (STXM) at BL 5.3.2 [1,2] offer the opportunity to obtain this data. We report here our first, and successful attempt at this kind of measurement.

RESULTS AND DISCUSSION

The absorption intensity in near edge x-ray absorption (NEXAFS) is determined by the projection of the transition dipole moment operator onto the electric field vector of the light. Thus, polymer orientation can be determined from the change in transition intensity as a function of sample angle [3]. In polystyrene, the C 1s $\rightarrow \pi^*_{ring}$ transition at 285.2 eV is oriented perpendicular to the ring. Since the ring planes are approximately perpendicular to the polymer axis [4] the polarization dependence of the strong 285.2 eV resonance is a convenient monitor of molecular orientation. In principle, one can quantify degree of polymer alignment by comparing the NEXAFS spectrum measured with the fibril axis aligned along the photon E vector, with that measured with the sample positioned at 90º to that orientation. In practice, this is very challenging since sample rotation in the STXM is difficult, the E-vector cannot be rotated (yet) [5], and since the fibrils are known from transmission electron microscopy (TEM) to be about 10-40 nm in diameter, somewhat smaller than the ~50 nm resolution of the STXM [2].

Another issue that needs to be considered is the possibility of beam damage caused by the measurement [6]. Early attempts to record the NEXAFS spectra of the matrix and the fibrils by using image spectral sequences [7] did in fact suffer from detectable damage, which in the case of PS has been shown to occur by degradation of the π^*_{ring} resonance [6]. To avoid that, we report here an approach resulting in the lowest possible damage.

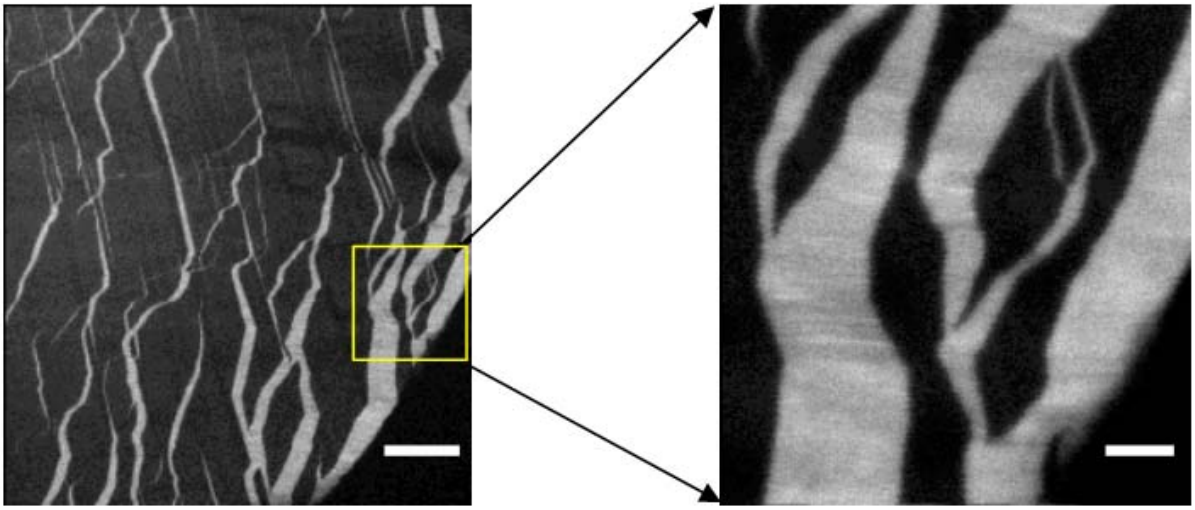

Fig. 1 STXM images at 285.2 eV of crazed PS. The image on the right was the crazed region used for dichroism measurements. Scale bars: left: 5 microns, right: 1 micron.

A microtomed thin section of general purpose PS (molecular weight approximately 100,000 Daltons) was placed on a copper TEM grid which had been pre-treated with an adhesive. A miniature deformation stage was used to stretch the grid and thereby stretch the PS section until crazes had formed. This process was monitored using a visible light microscope. This sample was then analyzed in the STXM.

Images measured at 285.2 eV are reproduced at two different magnifications in Figure 1. The lighter areas are the crazes and the darker material is the intact bulk PS. Although the fibrils are not completely resolved, their presence is discerned by the irregular haziness of the space between the dark regions of bulk PS. Two images were acquired per orientation set. The first image was at 285.2 eV, the top of the π^*_{ring} resonance, labelled A in Figure 2. The second image was acquired at 320 eV, labelled B in Figure 2, an energy well away from any absorption resonance, where variations in the carbon thickness are the only contrast mechanism. This was used to correct for the thickness differences between matrix and crazes as described below.

Both images were converted to optical density OD = -ln (I/Io), where I is the signal being detected through the sample in transmission and Io is the incident beam intensity. To compensate for density differences and thereby allow using the bulk PS as a reference, we have normalized the 285.2 eV images by dividing them by the 320 eV images. The image ratios for the fibrils oriented approximately parallel (horizontal) and perpendicular (vertical) to the electric vector of the photon field are compared in Figure 3. One sees that the fibrils in the crazes are brighter than the matrix when the E vector (in the horizontal plane of the image) is parallel to the fibrils. When the sample is rotated by 90^o to put the E vector perpendicular to the fibril direction, the craze region is much

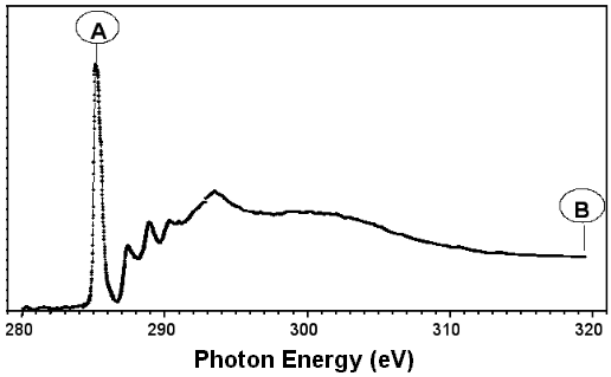

Fig. 2 C 1s spectrum of polystyrene. A and B indicate the energies where images were recorded to determine orientation.

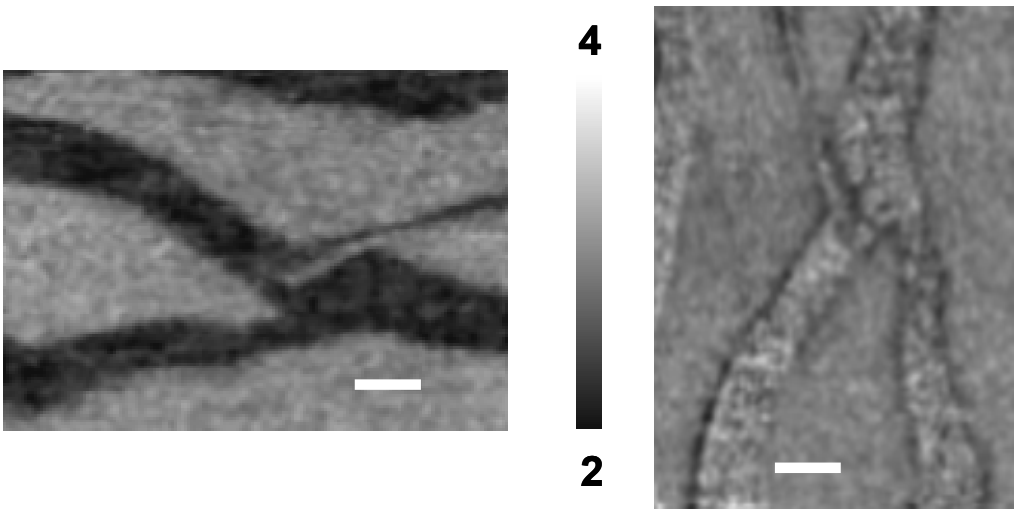

Fig. 3 Ratio of images at 285.2 and 320 eV. (left) sample with the crazes approximately parallel to E-vector (fibrils perpendicular to E-vector). (right) orthogonal sample orientation, craze perpendicular, fibrils parallel to E-vector. Bar is 1 micron.

darker compared to the matrix. These observations are consistent with the hypothesis that the fibrils are oriented PS chains across the crazes, with the phenyl rings approximately perpendicular to the fibril axis, and thus parallel to the craze. In this orientation, the E-vector should be perpendicular to the craze direction for maximum intensity of the C 1s → π^*_{ring} (Fig. 4), consistent with the observation (Fig. 3). In order to quantify the degree of orientation one needs to correct for the open area around the fibrils which 'dilutes' the dichroic signal.

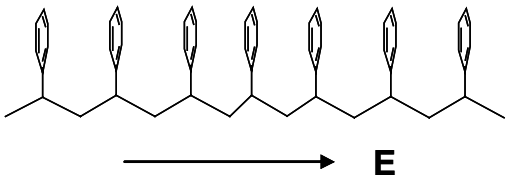

Fig. 4 Sketch to illustrate the suggested orientation of phenyl rings relative to the chain axis. The rings are all shown on the same side and the zigzag planar structure is used only for simplicity.

SUMMARY

NEXAFS dichroism has been used for the first time to directly confirm the orientation of molecular chains within fibrils in crazed polymers. Further experiments are planned to make more quantitative measurements and to study more complex polymeric systems. The information gleaned from these studies will contribute to our understanding of fracture properties of materials at a very fundamental and microscopic level.

REFERENCES

1. T. Warwick et al., J. Synchrotron Radiation (2002) submitted.
2. A.L.D. Kilcoyne et al., J. Synchrotron Radiation (2002) to be submitted..
3. J. Stöhr, *NEXAFS Spectroscopy*, Springer-Verlag, Berlin, 1992.
4. D. Fischer, G. Mitchell, A. Yeh, and J. Gland, Applied Surface Science 133 (1988) 58.
5. A.T. Young et al. J. Synchrotron Radiation (2002) submitted.
6. T. Coffey, S. G. Urquhart and H. Ade, J. Electron Spectroscopy and Related Phenomena, 122 (2002) 65.
7. T. Warwick et al., Journal of Synchrotron Radiation, 5 (1998) 1090.

This work was supported by The Dow Chemical Company.

Contact: Gary Mitchell, Dow Chemical, V: 989 636-3666, email: gemitchell@dow.com

Resonant Small Angle X-Ray Scattering of Polymers at the C-K edge

Ivaylo Koprinarov[1], Gary Mitchell[2], Brian Landes[2], Mike Devon[3] and Jeff Kortright[4]
[1]BIMR, McMaster University, Hamilton, ON, Canada L8S 4M1
[2]Analytical Sciences, The Dow Chemical Company, 1897 Building, Midland, MI, 48667
[3]Emulsion Polymers Research, The Dow Chemical Company, 1604 Building, Midland, MI 48667
[4]Lawrence Berkeley National Lab, Berkeley, CA 94720

INTRODUCTION

Small-angle x-ray scattering is a very valuable technique which complements microscopic techniques by providing statistically averaged information on polymer morphology. For the hard x-rays, scattering intensity is determined by the electron density contrast between two phases [1]. There are situations where this contrast mechanism is not sufficient, e.g. the case where the material has more than two phases or the electron density contrast is not sufficient to give detectable scattering.

We have begun a program to use resonant scattering energies to enhance the information content and signal to noise ratios in small angle x-ray scattering of polymers. Resonant x-ray scattering is a well known phenomenon and has been demonstrated for hard x-ray energies [2], but to our knowledge has never been attempted at the C1s edge, although it has been applied to study magnetic materials [3]. The soft x-ray energy places fairly formidable restrictions on sample preparation conditions. We have performed proof of principle experiments using latex polymers made from polystyrene and polymethylmethacrylate. The early results are very exciting and indicate that this technique may have several interesting and useful applications in the field of polymer characterization.

The x-ray scattering amplitude (f) is a function of energy and is a complex number and the imaginary part (f_2) is due to absorption [4]:

$$f(E) = f_1(E) + i f_2(E) \quad (1)$$

$$f_2(E) = \frac{\sigma_a(E)}{2 r_e \lambda} \quad (2)$$

$$f_1(E) = Z + \frac{1}{\pi r_e hc} \int_0^{\infty} \frac{\varepsilon^2 - \sigma_a(\varepsilon)}{E^2 - \varepsilon^2} \, d\varepsilon \quad (3)$$

The Kramer's Kronig dispersion relation relates the real and imaginary parts, where σ_a is the absorption cross section, λ is the wavelength, r_e is the classical electron radius, h is Planck's constant, c is the speed of light and Z is the atomic number.

Well away from an absorption resonance ($\sigma_a \Rightarrow 0$), x-ray scattering intensity (f^2) is determined by the electron density contrast between the (difference in Z) phases, as mentioned above. Near resonance, however, the intensity is modulated by the absorption cross section. Thus we can make use of the very same near edge x-ray absorption spectral features that have proven useful in x-ray microscopy [5], so-called *near-edge x-ray absorption fine structure* (NEXAFS) [6], to provide chemical contrast between different phases in a polymer system for small angle x-ray scattering experiments. The spectroscopic features, correspond to electronic excited states in which an inner-shell electron has been excited to unfilled molecular orbitals or conduction bands. They are determined by the bonding environment and thus provide a characteristic signature for every material.

The selective enhancement or suppression of the scattering in connection with chemical differences was demonstrated for the carbon C K-edge by using latex spheres of two different chemical compositions (polystyrene and polymethyl methacrylate; PS and PMMA respectively). These lattices were also of different sizes (80nm for PS and 300 nm for the PMMA). In figure 1 we have plotted the scattering intensity (the square of the scattering factor) for the PS and PMMA, calculated from the absorption spectra, using the relationships in equations 1-3.

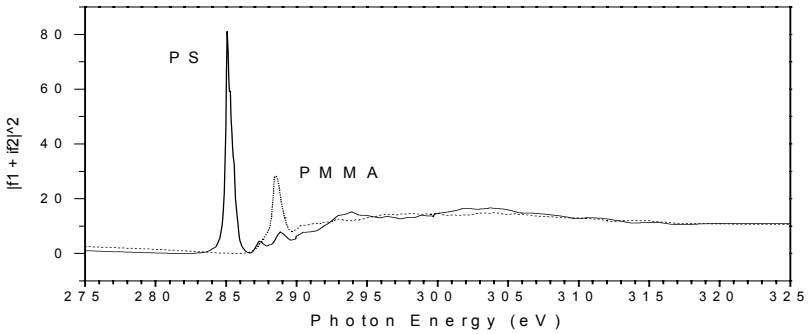

Figure 1. Scattering intensity (f^2) of PMMA and PS calculated from the measured NEXAFS spectra.

RESULTS AND DISCUSSION

NEAXFS spectra were measured from thin films of the lattices dispersed onto thin (100nm) Si_3N_4 windows using the BL7.0.1 scanning transmission x-ray microscope. The most intense peak for both materials is the C1s --> π^* transition which is associated with C=C bonds in PS and C=O bonds in PMMA. Fortuitously, the weakest scattering for each material occurs at energies just below the maximum intensity peak. In Figure 2 the scattering intensity as a function of scattering vector ($q = (4\pi/\lambda)\sin\theta$; θ = scattering angle) is plotted for PS and PMMA samples at the energies for minimum and maximum scattering intensities in each case. The patterns indeed show strong oscillations when measured at the peak scattering intensity and are relatively featureless at the energy of the minimum. In agreement with the relative sizes of the latex particles, one observes that the features in the scattering pattern for PMMA begin at lower q than those for the PS latex. The data can be analyzed by fitting to calculated scattering curves (not shown) and when this is done one retrieves information on particle size consistent with the data provided by the manufacturer measured by other methods. It is interesting to note that deviation of the experimentally acquired data from the calculated pattern occurs and can likely be attributed to the important interfacial or superficial structure of the lattices. This aspect of the data analysis is still under scrutiny by us.

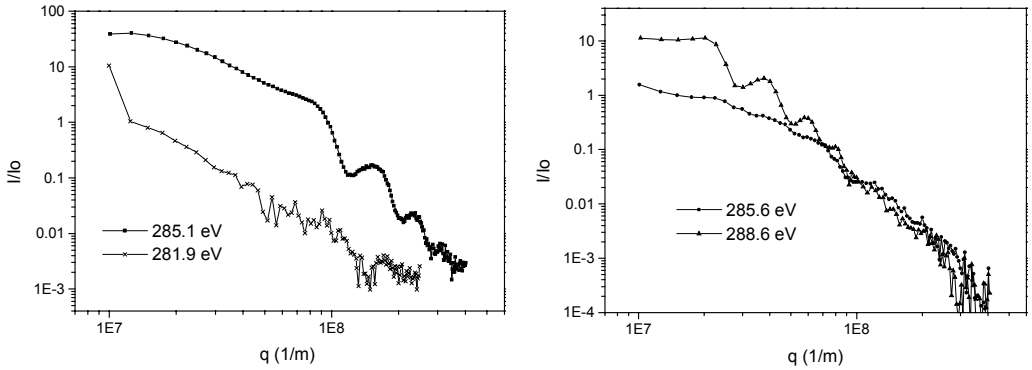

Figure 2. Scattering patterns measured as a function of q for PMMA latex spheres nominally 80 nm in diameter (right) and PS latex spheres nominally 300 nm in diameter (right).

In another experiment, samples of both of the two lattices were randomly dispersed (dried) onto the same Si_3N_4 window. This experiment demonstrates one powerful aspect of this polymer characterization method. When the scattering pattern is measured at 260 eV, well away from any absorption resonances, it appears to be a sum of scattering from both phases. However, at 281.9 eV the scattering from the PS spheres is suppressed and the pattern is dominated by features due to the PMMA spheres. On the other hand, when the data is measured with a photon energy of 285.6 eV the PMMA scattering is suppressed and the pattern is dominated by scattering from PS spheres. Figure 3 shows that in order to determine the structure of one material in the presence of the other, one may acquire the scattering patterns at the energies at which scattering from one phase and then the other phase is enhanced.

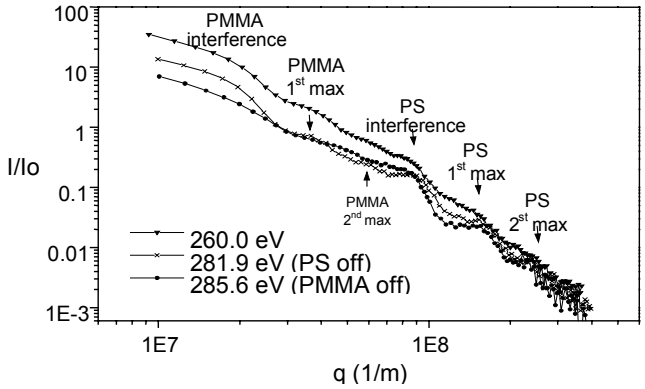

Figure 3. Scattering patterns measured as a function of q for a mixture of the PS latex spheres, nominally 80 nm in diameter and PMMA latex spheres, nominally 300 nm in diameter acquired at the indicated photon energies.

SUMMARY

The presented experiment combines the power of small-angle scattering for sub microscopic structural information with the carbon near-edge absorption fine structure as contrast mechanism for chemical composition. This approach is believed to be useful in several areas where multiphase material are being studied, including polymer blends, structured lattices, soft organic based colloidal materials, advanced electronic materials, structured compound materials, multiphase systems, and nanocomposites.

REFERENCES

1. A. Guinier, Ann. phys. 12, 161 (1939).
2. H. B. Stuhrmann, "Resonance Scattering in Macromolecular Structure Research", in "Advances in Polymer Science" vol. 67 edited by H. Kausch and H. Zachmann, 123-163 Springer-Verlag, Berlin (1985).
3. J. B. Kortright and Sang-Kong Kim, Physical Review B, 62 (2000) 12 216.
4. D. Atwood, "Soft X-Rays and Extreme Ultraviolet Radiation Principles and Applications", Cambrideg University Press, (1999)90-94.
5. H. Ade and S. G. Urquhart, "NEXAFS Spectroscopy and Microscopy of Natural and Synthetic Polymers", In *Chemical Applications of Synchrotron Radiation*, T. K. Sham, Ed. (World Scientific Publishing, Singapore, to be published.
6. J. Stöhr, *NEXAFS Spectroscopy*, Springer-Verlag, Berlin, 1992.

This work was supported by The Dow Chemical Company. One of us (JK) was supported by the Director, Office of Science, Office of Basic Energy Sciences of the U. S. Department of Energy under Contract No. DE-AC0376SF00098.

Contact: Gary Mitchell, Dow Chemical, V: 989 636-3666, email: gemitchell@dow.com

Spectroscopic observation of polaron-lattice band structure in the conducting polymer polyaniline

E.Z. Kurmaev[1], M.I. Katsnelson[1], A. Moewes[2], M. Magnuson[3], J.-H. Guo[3], S.M. Butorin[3], J. Nordgren[3], D.L. Ederer[4], and M. Iwami[5]

[1]Institute of Metal Physics, Russian Academy of Sciences-Ural Division, 620219 Yekaterinburg GSP-170, Russia
[2]University of Saskatchewan, Department of Physics and Engineering Physics, Saskatoon, SK S7N 5E2, Canada
[3]Department of Physics, Uppsala University, Uppsala, P.O. Box 530, S-75 121, Sweden
[4]Department of Physics, Tulane University, New Orleans, LA 70118, USA
[5]Research Laboratory for Surface Science, Okayama University, Okayama 700-8530, Japan

Interest in polyanilines has been reinforced by the discovery of their high electrical conductivity observed in doped phases, giving rise to a new class of conducting polymers. Polyaniline can be prepared in three major forms that differ in the degree of oxidation *y* (the ratio of amine nitrogens over the total number of nitrogen atoms). For the fully reduced leucoemeraldine base (LEB) *y* is one, the half-oxidized emeraldine base (EB) *y* is 0.5 and for fully oxidized pernigraniline base (PNB) *y* is 0. Polyaniline is an insulator in each of these forms with a band gap of 3.6 eV for LEB and EB and about 1.4 eV for PNB. The polymers can also exist in the corresponding protonated (salt) forms but only emeraldine salt (ES) is highly electrically conductive in this case. The largest conductivity reported to date is about 400 S/cm [1], which is 14 orders of magnitude higher than for the insulating emeraldine base form. Protonation does not change the electronic concentration and a local distortion of the chemical bonds is giving rise to conductivity of the polymer. These distortions are commonly referred to as either a polaron (storing the extra positive charge when only one nitrogen is protonated) or a bipolaron (in the case that both imine nitrogens are protonated). In order to explain the conductive state of ES two models have been proposed. A regular distribution of polarons leaves the electronic band half-filled or the random bipolaron structure leads to the formation of extended electronic states at the Fermi energy. There is no direct spectroscopic evidence to date regarding the electronic structure of ES, which is essential for selecting the adequate picture.

We have studied the differences in the electronic structure of protonated and undoped polyemeraldine by means of soft x-ray emission spectroscopy (XES). Our findings support the application of the polaronic-metal model for highly conducting polymers.

The experiments were carried out at Beamlines 7.0 and 8.0.1 at the Advanced Light Source at the Lawrence Berkeley National Laboratory employing the Uppsala University [3] and University of Tennessee at Knoxville [4] endstations. Photons with energies well above the carbon K-edge (300 eV) and well above the nitrogen K-edge (412-430 eV) were delivered to the sample. The X-ray fluorescence spectrometer provides an energy resolution of 0.30 eV and 0.65 eV for the carbon and nitrogen measurements, respectively. For our measurements we have chosen the basic form of undoped and protonated polyemeraldine. The doped samples were prepared by protonation with 60% camphorsulphonic acid (CSA). The protonation with H^+ adds holes to the imine groups around the quinoid ring.

Figure 1 shows carbon Kα emission spectra (2p→1s transition) of undoped and protonated emeraldine converted to the binding energy scale [5]. The spectra are normalized to the same peak height in the intensity maximum. The intensity of the C Kα emission in the vicinity of the Fermi level E_F is clearly increased for the protonated emeraldine compared to the undoped sample. This finite density of states at the Fermi level evidences the metallicity of the doped phase. The same tendency of higher spectral intensity in the vicinity of the Fermi level for protonated polyemeraldine with respect to the undoped phase is observed in N Kα XES though these measurements have been performed with less energy resolution (due to the higher emission energy) and lower count rate than the carbon data, the latter being due to the smaller content of nitrogen atoms in polyaniline. Protonating increases the finite density of states near the Fermi level and the origin of the increase is the formation of the polaron band. In the case of the bipolaron band structure no finite density of states is expected near E_F. Recently, an extremely small finite density of states for protonated emeraldine has been observed in photoemission measurements [6]. The authors do not indicate the level of protonation and in a protonation of too low concentration could lead to such effect.

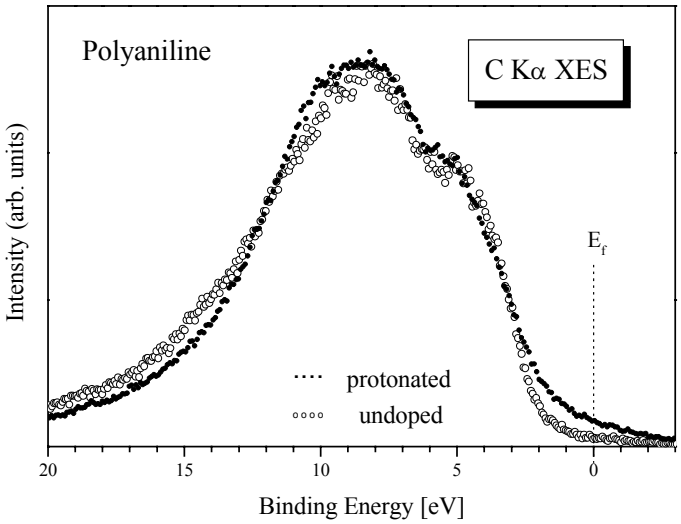

Figure 1 Carbon Kα XES of undoped and protonated polyemeraldine displayed on the binding energy scale.

To summarize, we have observed a finite density of states in protonated emeraldine in the vicinity of the Fermi level using soft X-ray emission measurements. This direct observation is in a full agreement with band structure calculations for the polaron lattice and therefore supports a polaronic-metal model for conducting polymers.

REFERENCES

1. M. Reghu, Y. Cao, D. Moses, and A.J. Heeger, Phys. Rev. B **47**, 1758 (1993).
2. S. Stafström, J.L. Bredas, A.J. Epstein, H.S. Woo, D.B. Tanner, W.S. Huang, and A.G. MacDiarmid, Phys. Rev. Lett. **59**, 1464 (1987).
3. J. Nordgren, G. Bray, S. Gramm, R. Nyholm, J.-E. Rubensson, and N. Wassdahl, Rev. Sci. Instrum. **60**, 1690 (1989).
4. J.J. Jia, T.A. Callcott, J. Yurkas, A. W.Ellis, F.J. Himpsel , M.G. Samant, J. Stöhr, D.L. Ederer, J.A. Carlisle, E.A. Hudson, L.J. Terminello, D.K. Shuh, and R.C.C. Perera, Rev. Sci. Instrum. 66 (1995) 1394.
5. E.Z. Kurmaev, M.I. Katsnelson, A. Moewes, M. Magnuson, J.-H. Guo, S.M. Butorin, J. Nordgren, D.L. Ederer and M. Iwami, J. Phys: Condens. Matter 13 (2001) 3907.
6. H.Sakamoto, M. Itow, N. Kachi, T. Kawahara, K. Mizoguchi, H. Ishii, T. Miyahara, K. Yoshioka, S. Masubuchi, S. Kazama, T. Matsushita, A. Sekiyama and S. Suga, J. Electr. Spectr. Relat. Phenom. **92**, 159 (1998).

This work was supported by the Russian State Program on Superconductivity, the Russian Science Foundation for Fundamental Research (Projects 00-15-96575 and 99-03-32503), the Swedish National Science Research Council (NFR), the Goran Gustavsson Foundation for Research in Natural Sciences and Medicine, NSF Grants DMR-901 7997 and DMR-9420425, the DOE EPSCOR and the Louisiana Education Quality Special Fund (DOE-LEQSF (1993-95-03)). The ALS, Lawrence Berkeley National Laboratory is supported by the U.S. Department of Energy under Contract No. DE-AC03-76SF 00098.

Principal investigator: Ernst Kurmaev, Institute of Metal Physics, Russian Academy of Sciences-Ural Division, 620219 Yekaterinburg GSP-170, Russia. Email: kurmaev@ifmlrs.uran.ru. Telephone: +7-3432-744183.

Status of the 5.3.2 bend magnet polymer STXM

David Kilcoyne[1], Harald Ade[1], Tolek Tyliszczak[2], A. Peter Hitchcock[2], Adam P. Hitchcock[2], E.G. Rightor[3], G.E. Mitchell[3], Mike Kritscher[4], Tony Warwick[4], Keith Franck[4], Erik Anderson[5]

[1]Dept. of Physics, North Carolina State University, Raleigh, NC 27695
[2]BIMR, McMaster University, Hamilton, ON, Canada L8S 4M1
[3]Dow Chemical, 1897 Bldg, Midland, MI 48667
[4]Advanced Light Source, Berkeley Lab, Berkeley, CA 94720
[5]Center for X-ray Optics, Berkeley Lab, Berkeley, CA 94720

INTRODUCTION

Over the past three years a qualitatively new design of Scanning Transmission X-ray Microscope (STXM) has been conceived, built and commissioned at beamline 5.3.2 at the ALS. A dramatic improvement in performance has been achieved by introducing laser interferometry to control the positioning of microscope components with an accuracy consistent with the optical resolution of the instrument, currently about 40 nm. The interferometer is a great advance over previous systems such as the old BL7.0 STXM at the ALS and the Stony Brook STXM at the NSLS. In the latter instruments, one could image at a fixed photon energy with a spatial resolution close to the diffraction limit of the zone plate utilized, but it was not possible to change the photon energy while maintaining the focused X-ray spot on the same place on a sample, or to image at successive energies over the same x-y frame. Hence, the spatial resolution was effectively degraded for chemical analysis. Over a typical C 1s NEXAFS scan from 280 to 320 eV the focal length changes by up to 300 μm, requiring displacement of the zone plate along the X-ray beam by this amount while simultaneously maintaining the lateral position of the zone plate relative to the sample with <20 nm precision. Mechanical systems achieving the required linearity of $>10^4$ are exceptional, and indeed, the experience at both the ALS and NSLS microscopes has been that spatial resolution in point spectral mode is rarely better than 200 nm and that one needs to use software to correct for image-to-image misalignment, with concomitant residual resolution degradation.

EXPERIMENTAL

The solution that has been developed by a team from several institutions, adopted for both the 5.3.2 STXM and the 7.0 upgrade with somewhat different implementation, is to introduce a 2-d laser interferometer which continuously monitors the relative (x,y) position of the zone plate and the sample (see **Fig 1**). In the 5.3.2 STXM the interferometer is used as part of the feedback control loop for the PI piezo fast scan stage which is used to position and scan the sample when making images. This system provides stability of

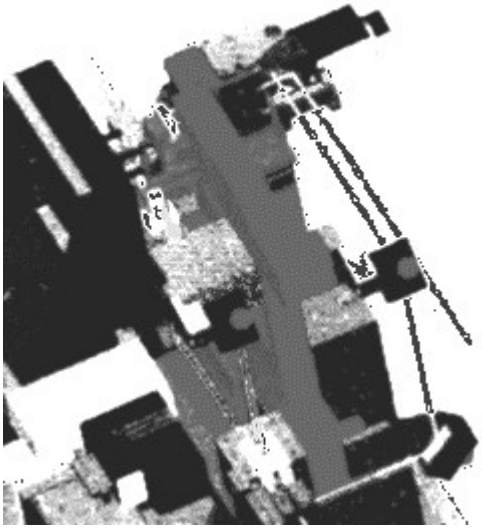

Fig. 1. View of the sample and zone plate stage region of the 5.3.2 STXM showing the paths of the laser beams used for 2-d interferometric control of relative position of the sample and the focused light.

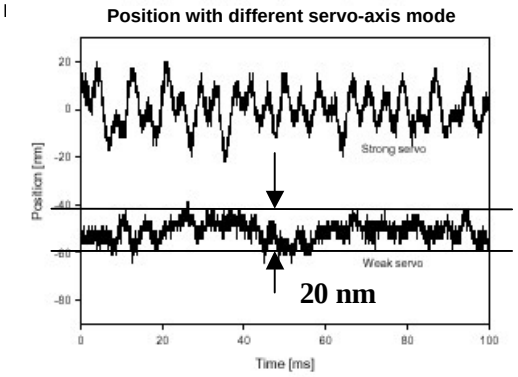

Fig. 2. Tests of positional stability over time of the sample position when under interferometric control (Tyliszczak, Feb-01)

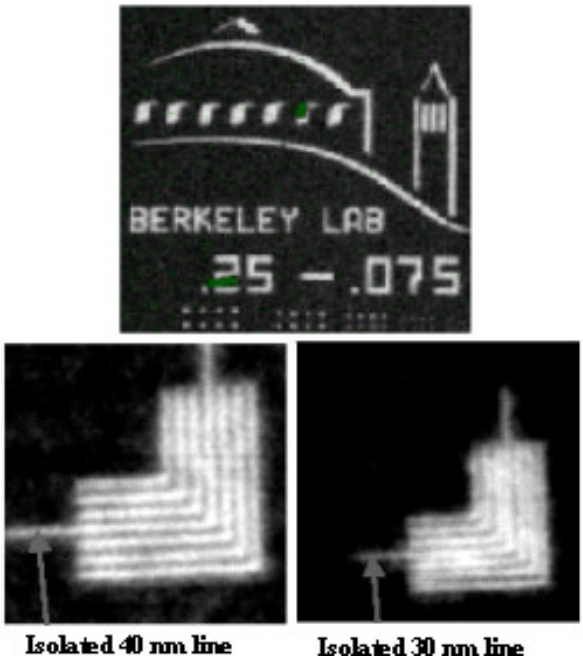

Fig. 3. Resolution tests using 1:1 Au lines on a silicon nitride substrate. The 40 nm pattern is fully resolved; the 30 nm pattern is partially resolved. (Each pattern consists of alternating lines and spaces of 30 or 40 nm). Zone plate and test pattern prepared by Erik Anderson *et al.* (CXRO, LBNL)

better than 20 nm with response times up to 100 Hz (see **Fig 2**) and thus it not only eliminates energy-to-energy image position errors, but also helps to desensitize the microscope to vibrational or other environmental noise.

With this mechanical/optical/control system, accompanied by advanced control and acquisition software, as well as excellent performance of the 5.3.2 spherical grating monochromator beamline [1], the 5.3.2 STXM is able to achieve diffraction limited spatial resolution. The images of a Au test pattern (**Fig 3**) indicate a spatial resolution of better than 40 nm, which is the theoretical diffraction limited resolution of the zone plate used. More significantly for analytical applications, the interferometry allows the 5.3.2 microscope to retain image registry at all photon energies. As an example of the level of positional stability achieved with the interferometry system, **Fig. 4** compares a linescan data set acquired at BL 5.3.2 in August 2001 on a polyurethane sample containing nanoscale filler particle with a data set on a similar sample recorded over a similar spatial and photon energy range, acquired with the old ALS beamline 7.0 STXM. In each case the raw data - position along line versus photon energy - is plotted. Clearly the ability to determine the NEXAFS spectra at high spatial resolution is greatly enhanced by the improved performance of the 5.3.2 STXM.

Further work on both the beamline and the mechanical and controls system has further increased stability and reliability of the 5.3.2 STXM [2] relative to its performance when these test measurements were performed.

REFERENCES

1. T. Warwick, *et al.* J. Synchrotron Rad. Submitted Jan 2002.
2. A.L.D. Kilcoyne *et al.* J. Synchrotron Rad. In preparation

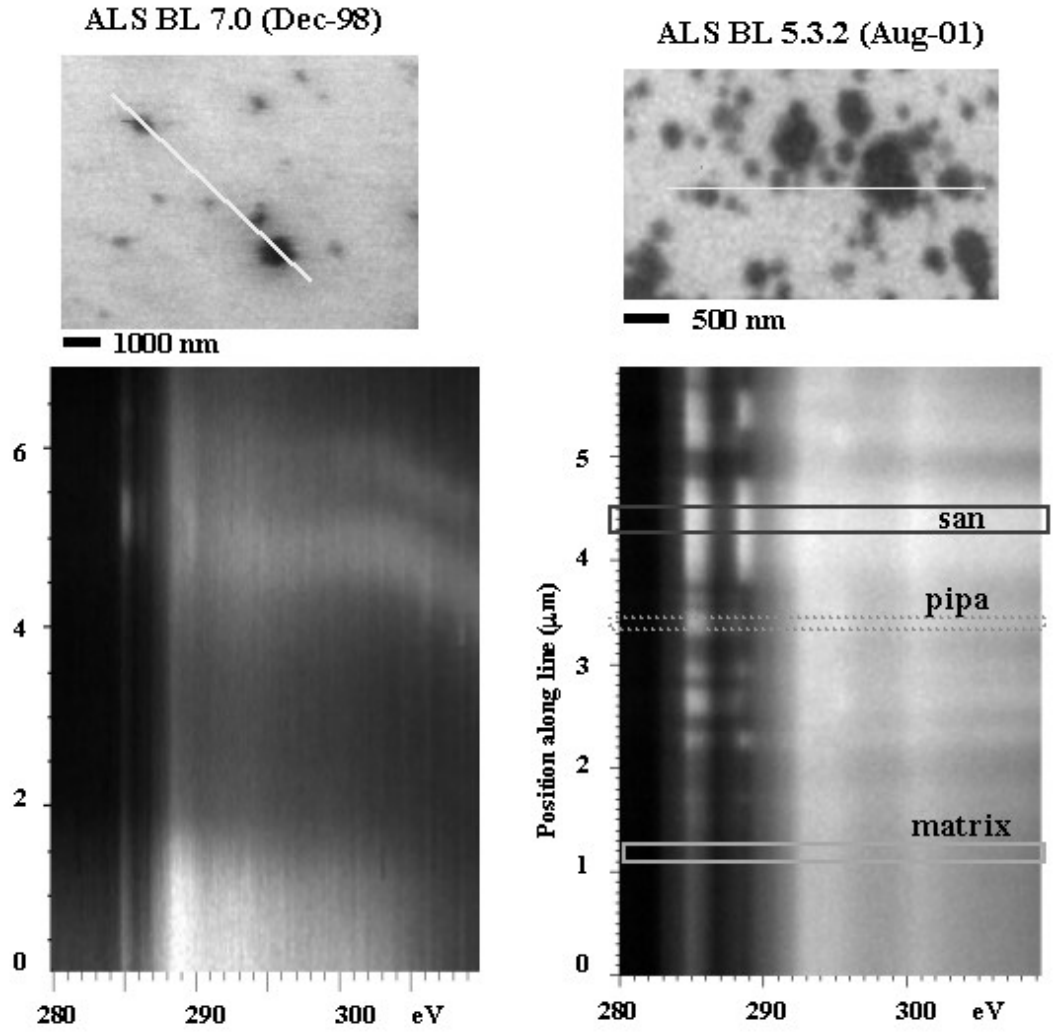

Fig. 4.
the old BL7.0 STXM and the new 5.3.2 STXM using data from filler particles (pipa) in a low-water polyurethane sample. The two lower 'images' plot 'linescans spectra' measured with each instrument. The display shows photon energy horizontally and position vertically - successive horizontal lines are the spectrum at pixels nominally along the line indicated in the true OD image of the samples displayed on the top (BL7.0: pipa only; BL5.3.2: pipa and san). The waviness of the signal in the horizontal direction in the left hand linescan is caused by drift of the X-ray spot on the sample due to mechanical limitations. In contrast, in the right hand linescan, there is negligible waviness in the horizontal direction. This is because the interferometric control in the 5.3.2 STXM provides precise zone plate - sample positioning at all photon energies. It also provides significant dynamic compensation for vibrations. Vibrations were present in the old 7.0 STXM and degraded its spatial resolution.

Capital costs for the beamline were provided by the ALS. Development costs for the STXM instrument were provided by DOE (DE-FG02-89ER60858), NSF (NSF DMR-9975694), the NSERC strategic program, Dow Chemical, and NCSU. The work of the McMaster group is supported by research and partnership grants from NSERC (Canada), the Canada Research Chair program (APH). The ALS is supported by the U.S. DOE, Office of Science.

Principal investigator: *Harald Ade*, NCSU, **harald_ade@ncsu.edu**. Ph: 919-515-1331

X-ray spectromicroscopy of branched polyolefin blends

G. Appel[1], I. Koprinarov[2], G.E. Mitchell[2], A.P. Smith[3] and H. Ade[1]

[1]Department of Physics, North Carolina State University, Raleigh, NC 27695
[2] Analytical Sciences, The Dow Chemical Company, 1897 Building, Midland, MI, 48667
[3]National Institute of Standards and Technology, Polymers Div., Gaithersburg, MD 20899

INTRODUCTION

It is generally difficult to determine the phase diagram of polyolefin blends directly by measuring the composition of phase separated domains. The constituent materials differ only in the amount and/or length of sidechains and provide little spectroscopic differences and limited contrast in traditional miroscopies [1-3]. Indirect methods to determine the phase diagram involve a large number of samples and elaborate contrast enhancement methods. Here, we explore the utility of Near Edge X-ray Absorption Fine Structure (NEXAFS) microscopy to determine polyolefin phase diagrams directly by determining the composition of phases in a limited number of samples. We have used the scanning transmission X-ray microscope (STXM) at beamline 7.0 to investigate thermally annealed blends of an ethylene-butene copolymer (EBC with 3.7 mol % butene) and of an ethylene-octene copolymer (EOC with 3.33 mol % octene). Despite the very similar chemical structure of these copolymers (they differ only in the length of the side chain, i.e. ethyl versus hexyl groups) NEXAFS microscopy can be used to a) directly visualize the morphology without staining or etching, and b) determine the composition of the phases in such blends.

EXPERIMENTAL

0.1 % m/m solutions of EBC and EOC (experimental polymer made with single site catalyst technology) in xylene were mixed in two different ratios (samples A1-4: 33%, samples C1-4 67% EOC). Subsequently, methanol was added to precipitate the polymer. The precipitate was collected by filtering and dried. The samples were vacuum-annealed at 180°C (samples A1, C1), 160°C (samples A2, C2), 140°C (samples A3, C3) and 120°C (samples A4, C4), respectively, quenched to -7°C and cryo-microtomed to about 100-200 nm in thickness.

The data were acquired at beamline 7.0.1. C1s-NEXAFS reference spectra of the pure components were derived from line-spectra (i.e. the same line scan at many photon energies). Image sequences of up to 80 images of small areas (typically 10 μm x 10 μm) as well as small series of large images (typically 6 images, 60 μm x 60 μm) were also recorded.

RESULTS AND DISCUSSION

The C1s-NEXAFS spectra of the two components are shown in Fig. 1. The most noticeable difference between both spectra is found in the 287-288eV energy region. EBC shows two closely spaced peaks (typical for linear polyethylene or polyolefins with few or short side-chains), EOC shows only one broad signal (typical for polyolefins with many or long side-chains). These signals are interpreted as σ^*(C-H) resonances [4]. Their spectral variations primarily reflect different intermolecular distances rather than different degrees of crystallinity. These spectra were used as reference spectra during the "stack fit" procedure [5] to determine the component maps.

Fig. 2 shows typical optical density (OD) images of two of the samples. The domains of the two phases can be clearly distinguished. Because EBC shows a higher absorption coefficient at 288.2eV than EOC (see Fig. 1), regions with high EBC concentration appear bright in Fig. 2b

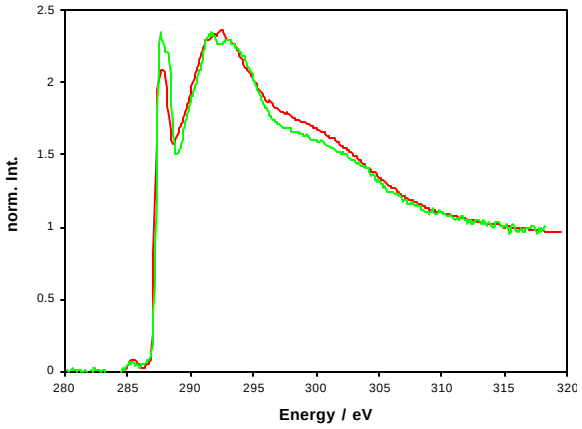

Fig. 1: C1s-NEXAFS reference spectra of the components: Red: ethylene-octene copolymer, green: ethylene-butene copolymer, both normalized to an edge jump of unity between 283eV and 315eV.

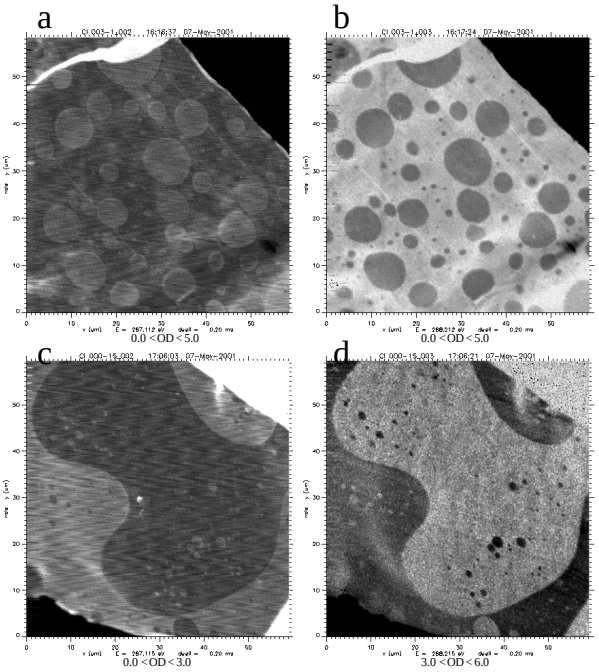

Fig. 2: Typical STXM optical density (OD) images of samples A3 (33% ethylene-octene copolymer): a), b) and C3 (67% ethylene-octene copolymer): c), d). Images a) and c) are taken at 287.1eV. Here domains, which are rich in the ethylene-octene copolymer appear bright. Images b) and d) are taken at 288.2eV and ethylene-butene rich domains appear bright in this case.

and 2d. At 287.1eV the opposite is the case and EOC rich regions appear bright. As expected from the ratio of the components in the mixed solutions, EBC forms the matrix- or majority-phase in sample A3 (a,b) and EOC in sample C3 (c,d).

After the images of an images sequence are aligned to correct for lateral shifts, the spectrum of each pixel in the stack area can be fitted by a linear combination of the reference spectra ($R_{oct}(E)$ and $R_{but}(E)$) and a constant, which is energy-independent (*constant*):

$$OD(E, x, y) = t_{oct}(x,y)*R_{oct}(E) + t_{but}(x,y)*R_{but}(E) + constant(x,y)$$

Thereby matrices of the effective thickness of the components $t_{oct}(x,y)$ and $t_{but}(x,y)$ and of the constant are determined and can be represented by component maps.

From these maps, regions in the matrix and in the minority phase were chosen carefully to not include inclusions of the other phase. Averaging over all pixels of these regions yields the effective thicknesses t. Since the sample contained only the two polymers, the composition Φ_{oct} (here the mass-fraction of EOC) can be calculated:

$$\Phi_{oct} = \frac{t_{oct}}{t_{oct} + t_{but}}$$

Thus, two composition values, one for the matrix and one for the minority phase, are derived for each sample. Fig. 3 shows these results for the different annealing temperatures. If we assume that the thermodynamical equilibrium was reached during the annealing and that the quenching conserved the composition of the melt, this diagram can be interpreted as a phase diagram. Although we presently estimate large errors (10-15%), an upper critical solution temperature behavior and a broad two-phase region is clearly visible.

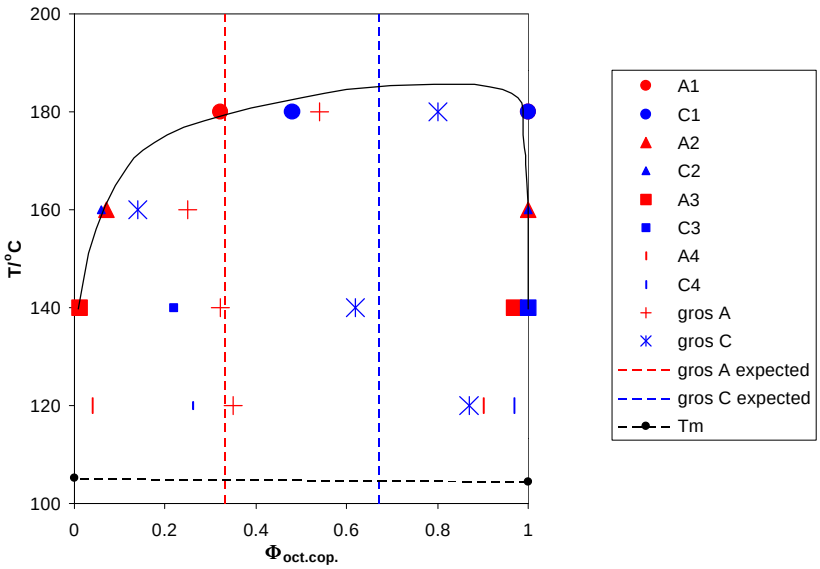

Fig. 3: Proposed phase diagram for the system poly(ethylene-ran-butene) – poly(ethylene-ran-octene). Small symbols were used, if the estimated reliability of the data was low. The gross amounts of the components from area weighted averages of the compositions and the gross amount expected from the preparation are indicated also.

In summary, we used NEXAFS-microscopy to determine the morphology and the composition of a specific polyolefin blend. The differences in the NEXAFS spectra of short- and long-branch copolymers provide sufficient image contrast, especially in the 287-288eV energy region, to image the morphology without further sample preparation (staining, etching). The polymers investigated show phase separation at all annealing temperatures. The matrix phase is always formed by the component that had the higher concentration in the solution and in the case of the EBC rich samples the gross sample composition is close to the solution composition. This indicates an almost quantitative precipitation by methanol. The phase diagram can be determined by quantitative evaluation of image sequences.

REFERENCES

1. M. J. Hill et al., Polymer **41,** 1621 (2000).
2. R. Krishnamoorti et al., J. Chem. Phys. **100,** 3894 (1994).
3. F. M. Mirabella Jr. et al., J. Polymer Sc. B 32, 2187 (1994).
4. A. Schoell A, R. Fink, E. Umbach, S. Urquhart, G.E. Mitchell, H. Ade, in preparation.
5. A. P. Hitchcock, AXIS2000 (Analysis of X-ray microscopy Images and Spectra).

This work was supported by DOE grant DE-FG02-98ER45737.

Principal investigator: Harald Ade, Department of Physics, North Carolina State University, Box 8202, Raleigh, NC 27695, e-mail: harald_ade@ncsu.edu, phone: 919 515 1331